Rapid Communications

Two-dimensional dynamics of elasto-inertial turbulence and its role in polymer drag reduction

S. Sid and V. E. Terrapon*
Department of Aerospace and Mechanical Engineering, University of Liège, Liège, Belgium

Y. Dubief
School of Engineering, University of Vermont, Vermont 05405, USA

(Received 4 October 2017; published 31 January 2018)

The goal of the present study is threefold: (i) to demonstrate the two-dimensional nature of the elasto-inertial instability in elasto-inertial turbulence (EIT), (ii) to identify the role of the bidimensional instability in three-dimensional EIT flows, and (iii) to establish the role of the small elastic scales in the mechanism of self-sustained EIT. Direct numerical simulations of viscoelastic fluid flows are performed in both two- and three-dimensional straight periodic channels using the Peterlin finitely extensible nonlinear elastic model (FENE-P). The Reynolds number is set to $\mathrm{Re}_\tau = 85$, which is subcritical for two-dimensional flows but beyond the transition for three-dimensional ones. The polymer properties selected correspond to those of typical dilute polymer solutions, and two moderate Weissenberg numbers, $\mathrm{Wi}_\tau = 40, 100$, are considered. The simulation results show that sustained turbulence can be observed in two-dimensional subcritical flows, confirming the existence of a bidimensional elasto-inertial instability. The same type of instability is also observed in three-dimensional simulations where both Newtonian and elasto-inertial turbulent structures coexist. Depending on the Wi number, one type of structure can dominate and drive the flow. For large Wi values, the elasto-inertial instability tends to prevail over the Newtonian turbulence. This statement is supported by (i) the absence of typical Newtonian near-wall vortices and (ii) strong similarities between two- and three-dimensional flows when considering larger Wi numbers. The role of small elastic scales is investigated by introducing global artificial diffusion (GAD) in the hyperbolic transport equation for polymers. The aim is to measure how the flow reacts when the smallest elastic scales are progressively filtered out. The study results show that the introduction of large polymer diffusion in the system strongly damps a significant part of the elastic scales that are necessary to feed turbulence, eventually leading to flow laminarization. A sufficiently high Schmidt number (weakly diffusive polymers) is necessary to allow self-sustained turbulence to settle. Although EIT can withstand a low amount of diffusion and remains in a nonlaminar chaotic state, adding a finite amount of GAD in the system can have an impact on the dynamics and lead to important quantitative changes, even for Schmidt numbers as large as 10^2. The use of GAD should therefore be avoided in viscoelastic flow simulations.

DOI: 10.1103/PhysRevFluids.3.011301

I. INTRODUCTION

The addition of small quantities of polymer macromolecules in wall-bounded flows is known to be one of the most efficient drag reduction strategies in turbulent flows [1]. Although great advances have

*vincent.terrapon@ulg.ac.be

 ©2018 American Physical Society

been made in the comprehension of the mechanism of polymer drag reduction, some key properties are still poorly understood. One is the longstanding question of the nature, Newtonian or Non-Newtonian, of the maximum drag reduction (MDR) state, observed by Virk [2]. A second, possibly related to the first, is the role of a recently discovered turbulent state, elasto-inertial turbulence (EIT) [3–5], in the dynamics of drag reduced flows. This Rapid Communication first focuses on the latter through an investigation of the dimensionality and role of small scale dynamics of EIT in channel flows at a marginally supercritical Reynolds number for three-dimensional flows. The findings then lend themselves to a discussion of the possible connection between EIT and MDR.

Concerted numerical and experimental research efforts in the last two decades have led to a solid understanding of how polymers reduce skin-friction drag in wall-bounded flows. The dampening of quasistreamwise vortices, the engine of wall turbulence [6], reported in many studies [7–10], arises from the stretching of polymers in the vertical motions caused by quasistreamwise vortices [11]; the stretched polymers work against these motions [12,13]. These advances owe a great deal to direct numerical simulation owing to a constitutive viscoelatic model, FENE-P (finitely extensible nonlinear elastic-Peterlin), which has been shown to capture the main dynamics of drag reduced flows with polymer additives.

Recently, the same model was at the center of the discovery of EIT. EIT [3–5] is a turbulent state driven by cyclic flow-polymer interactions, and can be found over a wide range of Reynolds numbers, from subcritical to supercritical. This polymer-driven turbulence is akin to elastic turbulence [14–16], a chaotic state found in inertial-less polymer flows undergoing curved mean streamlines. Beyond the sheer curiosity that the existence of EIT in parallel shear flows over a wide range of Reynolds number may elicit, the dynamical significance of EIT in polymer flows is yet to be established.

The first property is the dimensionality of EIT. Low Reynolds elastic turbulence has been previously observed in two-dimensional Kolmogorov flows [17], demonstrating the ability of elastic fluctuations to generate turbulence in two-dimensional (2D) planar shear flows. The coherent structures observed in three-dimensional (3D) EIT channel flows [3–5] also suggest that EIT may be 2D. Flow coherent structures depicted by the second invariant Q of the velocity gradient tensor are best described as cylindrical with a definite spanwise alignment, whereas the polymer field shows that stretched polymers are confined in sheets of large streamwise and spanwise scales and very small thickness in the wall-normal direction. EIT may be fundamentally two dimensional as the thin sheets seem to result from the stretching and the advection of polymers by the streamwise and wall-normal velocity components. If the two dimensionality of EIT is confirmed, it would imply that the underlying instability exists in three-dimensional flows and does not require any of the three-dimensional instabilities known in Newtonian flows to exist. In this Rapid Communication, we therefore conduct simulations in two and three dimensions for the same flow and polymer parameters in order to investigate the survival of EIT against Newtonian 3D instabilities.

The second focus of our study is the role of small scales in the dynamics of EIT. We have long suspected that small scales matter in turbulent polymer flows [18], however, it so far remains unclear whether the small scales of the polymer field have any significance to the dynamics of the flow and therefore to polymer drag reduction. The simulation of viscoelastic flows using the Eulerian framework is achieved by coupling the transport equation for the polymer conformation tensor to the Navier-Stokes equations. One important property of this transport equation is that there is no diffusive term, and terms other than the material derivative are not diffusive in nature [18]. Thus, from a mathematical point of view, the equation is hyperbolic. The absence of a diffusive term can be justified by the very low diffusion of polymers in solvents which has been reported to be of the order of 10^8 cm^2/s [19]. For dilute polymer solutions, it translates into Schmidt numbers (Sc), defined as the ratio between the solvent viscosity and the polymer molecular diffusivity, of the order of 10^6. The justifiable neglect represents a critical modeling challenge for the direct numerical simulation of polymer flows by making the transport equation a stiff hyperbolic problem. There are different approaches to solve this numerical challenge. The first is to add an artificial diffusive term to the transport equation to stabilize the simulation. However, a very low Schmidt number, Sc ≈ 0.5, has typically been used in practice [8,20–24]. The second is to guarantee that the conformation tensor

remains symmetric positive definite (SPD) during the simulation [25–28]. This approach is based on the Kurganov-Tadmor scheme [29] which dynamically adapts its order to maintain the SPD property at every grid point. The third relies on techniques used in compressible or multiphase flows to handle sharp discontinuities (shocks, gas-liquid interface) that attempt to add diffusion only in regions where gradients become too large to be solved on the local meshes [18,30]. This approach, akin to implicit large eddy simulations [18], allows one to model with higher fidelity the dynamics of $\mathrm{Sc} = \infty$ in the range of resolved scales. To date, the first method has not demonstrated an ability to simulate EIT, whereas EIT was discovered by the third one. The comparison between the two approaches sets the stage for a unique experiment to study the effects of small scales on EIT and polymer drag reduction by varying the Schmidt number.

According to the theory of passive scalar transport in turbulent flows [31,32], the smallest scalar scale is a function of the smallest scale of the flow and the Schmidt number. For a passive scalar in a turbulent flow of smallest scale η_K (Kolmogorov scale), the smallest scale of the scalar is the Obukhov-Corrsin scale $\eta_\mathrm{OC} = \eta_\mathrm{K}\mathrm{Sc}^{-3/4}$ when $\mathrm{Sc} < 1$, and the Batchelor scale $\eta_\mathrm{B} = \eta_\mathrm{K}\mathrm{Sc}^{-1/2}$ when $\mathrm{Sc} \gg 1$. Since polymers are not passive but actively scalar, one may not expect that Batchelor's theories directly and completely apply to our system. However, as discussed earlier [18], there is reasonable ground to anticipate that polymers should share some key dynamical features with a high Schmidt number scalar transport. Consequently, we study the range of Schmidt numbers over which EIT is observed and the effects of finite Schmidt numbers on the dynamics of the flow and polymer fields.

Finally, it is worth noting that particular care has been taken to ensure the quality of the results reported here. In order to verify the adequacy of the simulation methodology, two codes using different numerical schemes have been developed. The dynamical properties of the flows obtained using the two approaches have been compared through statistical distributions of the mean solvent velocity and polymer elongation. Moreover, a thorough mesh convergence study has been carried out to determine the spatial resolution necessary to properly capture all the relevant scales of the flow. The numerical analysis demonstrated that for a sufficiently fine grid, the solution is quasi-independent of the discretization for both finite and infinite Schmidt numbers. A discussion related to the accuracy of the simulation results is available in the Supplemental Material [33].

II. SIMULATION METHODOLOGY

Direct numerical simulations (DNS) of EIT are performed in two- and three-dimensional straight periodic channels for different flow conditions. The incompressible form of the Navier-Stokes equations coupled with a transport equation for the conformation tensor $\mathbf{C}$ are solved over the computational domain. The system can be written under its nondimensional form as

$$\nabla\cdot\mathbf{u} = 0, \quad \partial_t\mathbf{u} + \mathbf{u}\cdot\nabla\mathbf{u} = -\nabla p + \frac{\beta}{\mathrm{Re}_\tau}\nabla^2\mathbf{u} + \frac{1-\beta}{\mathrm{Re}_\tau}\nabla\cdot\boldsymbol{\tau}^p + f_x\mathbf{e}_x,$$
$$\partial_t\mathbf{C} + \mathbf{u}\cdot\nabla\mathbf{C} = \nabla\mathbf{u}\cdot\mathbf{C} + \mathbf{C}\cdot(\nabla\mathbf{u})^\mathrm{T} - \boldsymbol{\tau}^p + \frac{1}{\mathrm{Re}_\tau\mathrm{Sc}}\nabla^2\mathbf{C}, \tag{1}$$

where $\boldsymbol{\tau}^p$ is the polymer stress defined using the FENE-P model,

$$\boldsymbol{\tau}^p = \frac{1}{\mathrm{Wi}}\left[\frac{\mathbf{C}}{1-\mathrm{tr}(\mathbf{C})/L^2} - \mathbf{I}\right], \tag{2}$$

in which polymer molecules are modeled as dumbbells composed of two beads and a nonlinear spring. The conformation tensor $\mathbf{C} = \langle\mathbf{q}\otimes\mathbf{q}\rangle$ is defined as the local averaging of the tensor product between dimensionless end-to-end vectors $\mathbf{q}$ that characterize the orientation and the length of each dumbbell. The governing equations are controlled by five nondimensional parameters: the Reynolds number $\mathrm{Re}_\tau = u_\tau\delta/\nu$ based on the friction velocity u_τ, the half channel width δ, and the zero-shear-rate kinematic viscosity of the solution ν; the ratio between the solvent and solution viscosity $\beta = \nu^s/\nu$;

the Schmidt number $\mathrm{Sc} = \nu^s/\alpha$ defined as the ratio between the solvent kinematic viscosity ν^s and polymer diffusivity α; the Weissenberg number $\mathrm{Wi} = \lambda u_\tau/\delta$, which compares the polymer relaxation time λ to the wall shear rate of the corresponding Newtonian flow u_τ/δ; and the maximum dimensionless polymer extension L. Note that the viscous Weissenberg number defined as $\mathrm{Wi}_\tau = \mathrm{Wi}\,\mathrm{Re}_\tau = \lambda u_\tau^2/\nu$ is the one used here to define the flow conditions. The mean flow is driven by the body force $f_x\mathbf{e}_x$, which is a constant pressure gradient along the streamwise direction.

The nondimensional parameters selected for the study are the following: $\mathrm{Re}_\tau = 84.95$, $\beta = 0.97$, $L = 70.9, \mathrm{Wi}_\tau = [40, 100]$. A friction Reynolds number of $\mathrm{Re}_\tau = 84.95$ is on the lower end of the low Reynolds number turbulent regime for channel flows and just beyond the critical value of $\mathrm{Re}_{\tau,c} \approx 60$ for which Newtonian instabilities appear in three-dimensional flows. However, for two-dimensional channels, the critical bulk Reynolds number is approximatively $\mathrm{Re}_{b,c} \approx 5772$ [34], which is larger than a value of $\mathrm{Re}_b = 4817$ corresponding to $\mathrm{Re}_\tau = 85$. Lastly, the choice of Reynolds number, domain dimensions, resolution, and polymer parameters allows for a direct comparison with DNS of viscoelastic flows using $\mathrm{Sc} \leqslant 0.5$ [23,35,36].

The β parameter is selected in the typical range for dilute polymer solutions, and the maximum dimensionless polymer extension L is chosen sufficiently large to allow the solvent shear to stretch the polymer chains. The Schmidt number is set to infinite (no diffusive term) for the simulations used to investigate the elasto-inertial instability in order to prevent excessive polymer diffusion to affect the flow solution and allow all the relevant scales to freely develop. Respecting the hyperbolic nature of the polymer transport model is key to accurately simulate viscoelastic turbulence, as will be shown in the third part of the results section.

Viscoelastic flows are stable according to the linear stability theory [37]. Thus, an initial perturbation is necessary to trigger turbulence. The present methodology uses an alternated blowing-suction transverse excitation [4] added to the laminar viscoelastic Poiseuille flow during a short period of time to perturb the stable solution. After several flow-through times, the external excitation is turned off and the flow naturally develops towards its turbulent statistically steady state.

The channel length is chosen as long as possible to minimize possible numerical effects due to short-range interactions between highly stretched polymers through the periodic boundaries. A length of $L_x^+ = L_x u_\tau/\nu = 720$ is selected for all the simulations and three-dimensional simulations use a span of $L_z^+ = L_x u_\tau/\nu = 255$. It should be noted that EIT exists in domains with half the streamwise dimension of the present computational domain.

The numerical resolution of the system of equations (1) is performed using second-order finite difference schemes with a staggered variable arrangement [38,39] which ensures the discrete conservation of mass, momentum, and kinetic energy. The continuity equation is enforced through a fractional step method [40] where a Poisson equation for pressure is solved in the Fourier physical space. The system is advanced in time using the Crank-Nicholson semi-implicit scheme. As mentioned before, the choice of the discretization and the adequacy of the numerical methods have been verified using code comparison and a mesh sensitivity analysis that is reported in the Supplemental Material [33].

III. RESULTS

Figure 1 shows the instantaneous contours of polymer elongation observed in two-dimensional elasto-inertial turbulence at the statistically steady state. After a sufficiently long simulation time, the flow fully develops into a self-sustained chaotic motion. For the two Weissenberg numbers considered, the elastic and turbulent kinetic energies fluctuate around their mean values and do not show any sign of decay for more than 100 flow-through times (not shown here). The existence of a sustained turbulent motion in two-dimensional flows demonstrates the ability of FENE-P fluid flows to generate turbulence for a subcritical (2D) Reynolds number in wall-bounded planar configurations.

The physical mechanism behind the observed elasto-inertial instability is very similar to the one depicted in Ref. [4] for a similar range of Wi number in three-dimensional flows. Thin sheets of large polymer extensions arise from the stretching and the advection of polymer macromolecules

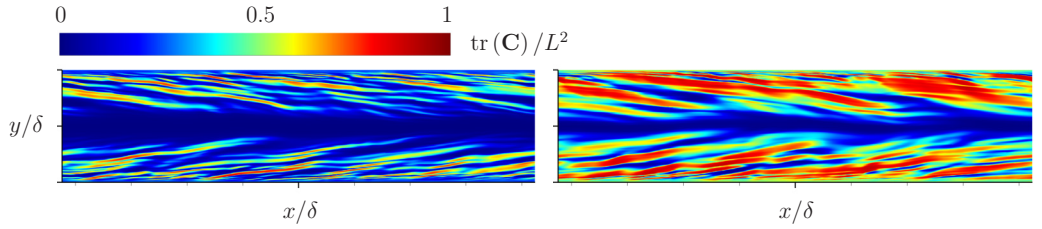


FIG. 1. Instantaneous contours of polymer elongation $\mathrm{tr}(\mathbf{C})/L^2$ in two-dimensional simulations. Left: $\mathrm{Wi}_\tau = 40$; right: $\mathrm{Wi}_\tau = 100$.

by the solvent. The accumulation of anisotropic elastic stress in the sheets, in turn, induces velocity fluctuations organized as a train of alternating circular regions of rotational and extensional topology. The flow inertia of this chaotic motion feeds the polymer stretching mechanism and regenerates the polymer sheets, closing the loop of self-sustained EIT. As the flow is confined in a two-dimensional channel and is thus subcritical, the typical Newtonian turbulent structures are not able to flourish and the dynamics is exclusively driven by the elasto-inertial instability. In fact, it has been shown that, for Newtonian fluids, reducing the channel span below a minimum size necessary to allow fundamental structures to develop hinders the cycle of near-wall turbulence and leads to the flow laminarization [6,41].

Comparing the two flow conditions indicates that, for the same level of solvent inertia (Reynolds number), increasing the Weissenberg number allows polymer chains to reach larger elongations over a wider fluid layer. In addition, the kinetic energy of momentum fluctuations also increases as the turbulent flow motion is sustained by the elastic stress gradients that are directly related to the local variations of polymer elongation. However, the dynamical behavior is very similar for the two Wi numbers considered.

The flow structures observed in three-dimensional channels for the same flow conditions are reported in Fig. 2. As the Reynolds number is supercritical for three-dimensional flows, the viscoelastic turbulence observed results from the interactions between Newtonian and elasto-inertial

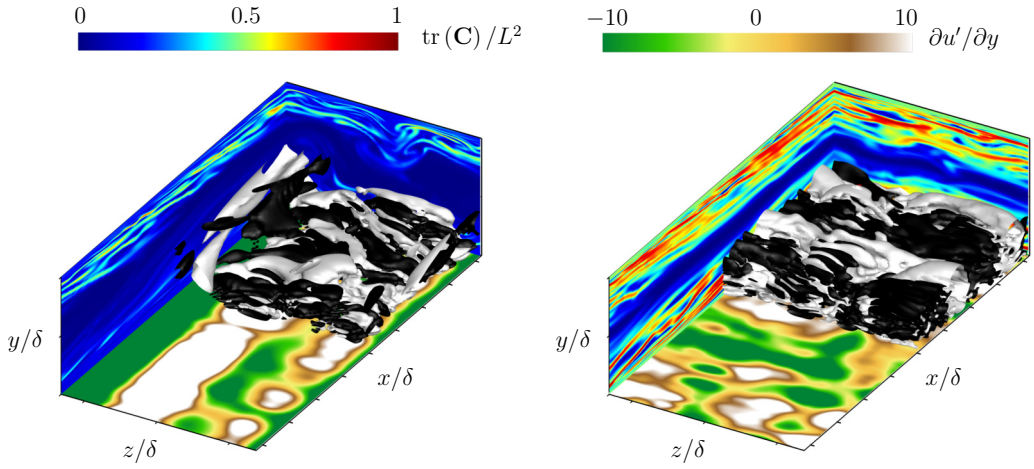


FIG. 2. Visualization of flow structures in three-dimensional flows. Contours of polymer elongation $\mathrm{tr}(\mathbf{C})/L^2$ in vertical planes, contours of streamwise shear fluctuations in a near-wall horizontal plane, and turbulent structures identified by large positive (white) and negative (black) Q-criterion values (only shown in the bottom half of the channel). Left: $\mathrm{Wi}_\tau = 40$; right: $\mathrm{Wi}_\tau = 100$.

turbulent structures. For the lower Weissenberg number, the two types of structures are clearly visible in the flow. The contours of polymer elongation in vertical planes show polymer sheet structures that are similar to those observed in two-dimensional flows. However, the sheets are not homogeneous along the channel span and are intermittently subject to the shear and advection of near-wall Newtonian vortices (see the vortical structure at the channel centerline near the top wall). These vortices are associated with long velocity streaks identified by large streamwise shear fluctuations. For the channel span selected, a single streak is observed in the flow. Despite the polymer-solvent interactions, the large streak colored in white remains coherent along the streamwise direction, demonstrating the relative importance of Newtonian turbulence at this Weissenberg number. The turbulent structures identified by positive values of the Q criterion [42] (rotational) also show that near-wall hairpin vortices are able to develop in the flow but are less frequent than in Newtonian turbulence. The spanwise aligned structures occupying a large part of the channel span correspond to the train of alternating circular regions of rotational and extensional topology specific to the elasto-inertial instability.

At larger Weissenberg numbers, the picture is relatively different. The Newtonian structures are no longer observed in the flow and the dynamics appears to be dominated by the elasto-inertial instability. Near-wall vortices and velocity streaks are inhibited by a stronger elasto-inertial turbulence. The streaks have lost their coherency and the only structures that can be observed are those specific to EIT. These structures are well organized and occupy the full channel span. The polymer sheets are homogeneous along the spanwise direction. Although additional fluctuations inherent to the extension to three-dimensional flows exist, large Wi EIT shares many dynamical features with two-dimensional elasto-inertial flows as this is the dominating instability. The similarities between two- and three-dimensional flows at larger Wi can also be measured quantitatively by comparing the power spectral density of the turbulence in the different flows. The averaged spectra analyzed are defined as

$$\overline{\langle \phi_{k,x} \rangle}_{\Omega} = \frac{1}{T_s}\frac{1}{\Omega}\int_{t_0}^{t_0+T_s}\int_{\Omega} \phi_{k,x}(\kappa_x, y, z, t)\, d\Omega\, dt,$$

with

$$\phi_{k,x}(\kappa_x, y, z, t) = \frac{1}{2u_\tau^2}[\hat{\mathbf{u}}(\kappa_x, y, z, t) \cdot \hat{\mathbf{u}}^*(\kappa_x, y, z, t)], \tag{3}$$

where T_s is the time averaging window, and Ω is the channel volume. The hat operator stands for the Fourier transform along the streamwise x direction, $\hat{\bullet} = \mathcal{F}_x(\bullet)$, and the superscript asterisk denotes the complex conjugate. These spectra are reported in the left panel of Fig. 3. The wave number κ_x is normalized by the wall Kolmogorov scale $\eta_K = (\nu^3/\epsilon_{\text{wall}})^{1/4}$ computed *a posteriori* from simulation results. One can see that for the larger Weissenberg number, the spectrum of the three-dimensional flow has a shape that is closer to the one obtained for the two-dimensional flow. The small-scale content increases with Wi and the slope of the inertial range tends to converge towards the one obtained for the two-dimensional flow. This additional comparison corroborates previous qualitative results and demonstrates the importance of the elasto-inertial instability in moderate/large Weissenberg number EIT.

The effects of the Schmidt number on the different scales of the turbulence can be evaluated in the right panel of Fig. 3. For the present conditions, a Schmidt number $\text{Sc} < 9$ leads to a complete laminarization of the flow. For $\text{Sc} \geqslant 9$, the range of scales affected is directly related to the amount of polymer diffusion introduced. A Schmidt number of $\text{Sc} = 100$ does not have a significant impact on the large scales and only damps a part of the sub-Kolmogorov scales. However, a wider range of scales is affected by the diffusion as the Schmidt number decreases. For values $9 \leqslant \text{Sc} < 100$, all the scales are diffused and the turbulent kinetic energy spectrum progressively narrows and weakens. It is important to emphasize that there is no universal minimum Schmidt number for which EIT is observed. The critical value depends on the numerical schemes used in the code as the effective

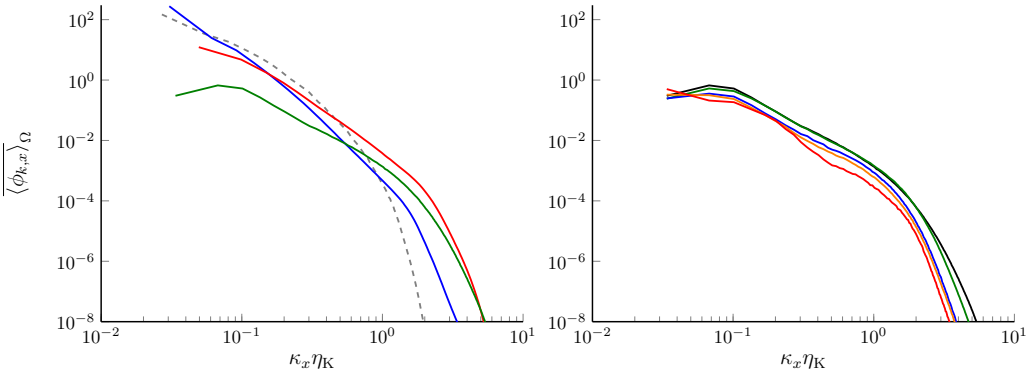


FIG. 3. Streamwise spectra of turbulent kinetic energy k averaged over the computational domain and over time. Left: Two- and three-dimensional flows at $\mathrm{Sc} = \infty$ for different Weissenberg numbers: (dashed gray) 3D, Newtonian; (blue) 3D, $\mathrm{Wi}_\tau = 40$; (red) 3D, $\mathrm{Wi}_\tau = 100$; and (green) 2D, $\mathrm{Wi}_\tau = 40$. Right: Two-dimensional flow at $\mathrm{Wi}_\tau = 40$ for different Schmidt numbers: (red) $\mathrm{Sc} = 9$; (orange) $\mathrm{Sc} = 16$; (blue) $\mathrm{Sc} = 25$; (green) $\mathrm{Sc} = 100$; and (black) $\mathrm{Sc} = \infty$.

dissipation results from the superposition of (i) the numerical dissipation of the schemes and (ii) the artificial dissipation introduced through the finite Schmidt number.

Additionally, the quantitative effects of an unrealistically large polymer diffusion on the mean velocity and polymer elongation profiles can be appreciated in Fig. 4. Lowering the Schmidt number increases the mean flow velocity and reduces the mean polymer extension. The diffusion tends to homogenize the elastic stress spatial distribution and counterbalance the stretching mechanism. Thus, diffusing the small-scale polymeric stress fluctuations of the sheets hinders the turbulence generation mechanism, leading to a reduction of the magnitude of the velocity fluctuations. As a consequence, the turbulent flow resistance is weakened and the flow rate increases. It is worth noting that diffusion has a double effect on polymer elongation. In addition to directly diffusing the highly stretched sheets, the reduced level of turbulence in the flow induces a depletion of the stretching mechanism by the solvent inertia.

More generally, excessive polymer diffusion tends to prevent elastic fluctuations to develop and therefore inhibits the elasto-inertial instability. As long as the diffusion is not too strong, the polymer

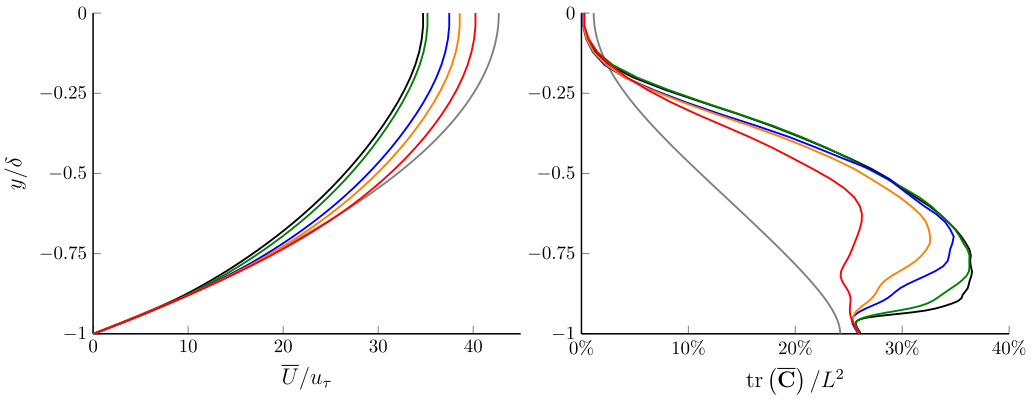


FIG. 4. Mean streamwise velocity profile (left) and mean polymer elongation profile (right) for a two-dimensional flow at $\mathrm{Wi}_\tau = 40$ and different Schmidt numbers: (gray) $\mathrm{Sc} = 0.5$ (laminar); (red) $\mathrm{Sc} = 9$; (orange) $\mathrm{Sc} = 16$; (blue) $\mathrm{Sc} = 25$; (green) $\mathrm{Sc} = 100$; and (black) $\mathrm{Sc} = \infty$.

stress gradients remain large enough to sustain the solvent chaotic motion necessary to regenerate the small-scale elastic sheets and preserve the global EIT dynamics. However, although turbulence is sustained under such conditions, the flow remains subject to an excessive spurious diffusion, even for high Schmidt numbers. A numerical procedure without GAD should therefore be preferred.

IV. CONCLUSION

The key outcomes of this investigation are that (i) EIT is fundamentally two dimensional, (ii) its inherent existence in three-dimensional flows overwhelms the dynamics, providing that the polymer solution is able to inhibit the growth of near-wall vortices through the polymer drag reduction mechanism, and (iii) the mechanism of EIT is small scales, as shown by the Schmidt number study. To further demonstrate outcome (ii), the present results can be compared to those of Wang *et al.* [43], who used the same Reynolds number, other polymer parameters, and a Schmidt number $\mathrm{Sc} = 0.5$. They reported intermediate drag reduction at $\mathrm{Wi}_\tau = 40$ and MDR at $\mathrm{Wi}_\tau = 100$, yet with flow structures that are clearly of a Newtonian nature. Our Schmidt number study demonstrates that EIT ceases to exist when $\mathrm{Sc} < 9$, yet for $\mathrm{Sc} = \infty$, streamwise vortices (a distinct feature of Newtonian turbulence) are only observed intermittently and only for $\mathrm{Wi}_\tau = 40$. For $\mathrm{Wi}_\tau = 100$, EIT is strong enough to fully dominate the dynamics of the flow. Note that the critical value of $\mathrm{Sc} = 9$ obtained in this study is not universal but specific to the numerical schemes used in the code.

The introduction of large polymer diffusion into the system damps a significant part of the elastic scales that are necessary to feed turbulence, eventually leading to flow laminarization. The transition to the laminar state does not systematically occur as EIT can withstand a low/moderate amount of diffusion without inhibiting the turbulence generation mechanism. Nevertheless, adding an unrealistically large polymer diffusion to the system has an important impact on the dynamics and leads to significant quantitative changes, even for Schmidt numbers as large as 10^2. This observation demonstrates the importance of the small elastic scales and highlights the necessity for preserving the hyperbolic nature of the transport equation by using zero-diffusion polymers. Outcome (iii) is critical for the understanding of polymer drag reduction and specifically MDR. Previous studies have concluded that the nature of MDR is Newtonian [23,35,36,43,44] for the same marginally critical Reynolds number. However, the present results suggest that their conclusion is biased by the use of numerical methods that dissipate the small-scale dynamics critical to EIT. Our study concludes that, for the Reynolds number considered here, MDR is EIT.

The extension to higher Reynolds number is not straightforward and will be the focus of future investigations. The authors speculate that EIT should dominate MDR, providing that polymer parameters are adequate in the range of Reynolds numbers for which the sustaining mechanism of wall turbulence is confined to the inner region, as shown by Jiménez and Pinelli [6]. For high Reynolds numbers, energy transfers between the outer and inner regions could compete and possibly dominate EIT.

ACKNOWLEDGMENTS

S.S. is grateful to the Fonds de la Recherche Scientifique (F.R.S.-FNRS) for funding the present research project. V.E.T. acknowledges the financial support of a Marie Curie FP7 Career Integration Grant (Grant No. PCIG10-GA-2011-304073) and of a grant from the "Fonds spéciaux pour la recherche" of the University of Liege (Crédits classiques 2013) (Grant No. C-13/19). Computational resources have been provided by the Consortium des Équipements de Calcul Intensif (CECI) funded by the Fonds de la Recherche Scientifique (F.R.S.-FNRS), the Vermont Advanced Computing Center (VACC), and the Partnership for Advanced Computing in Europe (PRACE) that are appreciatively acknowledged. The present research also benefited from computational resources made available on the Tier-1 supercomputer of the Fédération Wallonie-Bruxelles, infrastructure funded by the Walloon Region under Grant Agreement No. 117545. Y.D.'s contribution is supported by a National Science Foundation/Department of Energy Partnership Award No. 1258697.

[1] B. A. Toms, Some observations on the flow of linear polymer solutions through straight tubes at large Reynolds numbers, In Proc. 1st Intl. Congr. on Rheology **2**, 135 (1948).
[2] P. S. Virk, Drag reduction fundamentals, AIChE J. **21**, 625 (1975).
[3] D. Samanta, Y. Dubief, M. Holzner, C. Schäfer, A. N. Morozov, C. Wagner, and B. Hof, Elasto-inertial turbulence, Proc. Natl. Acad. Sci. USA **110**, 10557 (2013).
[4] Y. Dubief, V. E. Terrapon, and J. Soria, On the mechanism of elasto-inertial turbulence, Phys. Fluids **25**, 110817 (2013).
[5] V. E. Terrapon, Y. Dubief, and J. Soria, On the role of pressure in elasto-inertial turbulence, J. Turbul. **16**, 26 (2014).
[6] J. Jiménez and A. Pinelli, The autonomous cycle of near-wall turbulence, J. Fluid Mech. **389**, 335 (1999).
[7] C. D. Dimitropoulos, R. Sureshkumar, A. N. Beris, and R. Handler, Budgets of Reynolds stress, kinetic energy, and streamwise enstrophy in viscoelastic turbulent channel flow, Phys. Fluids **13**, 1016 (2001).
[8] P. K. Ptasinski, B. J. Boersma, F. T. M. Nieuwstadt, M. A. Hulsen, B .H. A. A. Van Den Brule, and J. C. R. Hunt, Turbulent channel flow near maximum drag reduction: Simulations, experiments and mechanisms, J. Fluid Mech. **490**, 251 (2003).
[9] T. Min, H. Choi, and J. Yul Yoo, Maximum drag reduction in a turbulent channel flow by polymer additives, J. Fluid Mech. **492**, 91 (2003).
[10] T. Min, J. Yul Yoo, H. Choi, and D. D. Joseph, Drag reduction by polymer additives in a turbulent channel flow, J. Fluid Mech. **486**, 213 (2003).
[11] V. E. Terrapon, Y. Dubief, P. Moin, E. S. G. Shaqfeh, and S. K. Lele, Simulated polymer stretch in a turbulent flow using Brownian dynamics, J. Fluid Mech. **504**, 61 (2004).
[12] Y. Dubief, C. M. White, V. E. Terrapon, E. S. G. Shaqfeh, P. Moin, and S. K. Lele, On the coherent drag-reducing and turbulence-enhancing behavior of polymers in wall flows, J. Fluid Mech. **514**, 271 (2004).
[13] K. Kim, R. J. Adrian, S. Balachandar, and R Sureshkumar, Dynamics of Hairpin Vortices and Polymer-Induced Turbulent Drag Reduction, Phys. Rev. Lett. **100**, 134504 (2008).
[14] A. Groisman and V. Steinberg, Elastic turbulence in a polymer solution flow, Nature (London) **405**, 53 (2000).
[15] A. Groisman and V. Steinberg, Efficient mixing at low Reynolds numbers using polymer additives, Nature (London) **410**, 905 (2001).
[16] A. Groisman and V. Steinberg, Elastic turbulence in curvilinear flows of polymer solutions, New J. Phys. **6**, 29 (2004).
[17] S. Berti and G. Boffetta, Elastic waves and transition to elastic turbulence in a two-dimensional viscoelastic Kolmogorov flow, Phys. Rev. E **82**, 036314 (2010).
[18] Y. Dubief, V. E. Terrapon, C. M. White, E. S. G. Shaqfeh, P. Moin, and S. K. Lele, New answers on the interaction between polymers and vortices in turbulent flows, Flow, Turbul. Combust. **74**, 311 (2005).
[19] Y. Layec and M.-N. Layec-Raphalen, Instability of dilute poly (ethylene-oxide) solutions, J. Phys. Lett. **44**, 121 (1983).
[20] R. Sureshkumar, A. N. Beris, and R. A. Handler, Direct numerical simulation of the turbulent channel flow of a polymer solution, Phys. Fluids **9**, 743 (1997).
[21] E. De Angelis, C. M. Casciola, V. S. L'vov, R. Piva, and I. Procaccia, Drag reduction by polymers in turbulent channel flows: Energy redistribution between invariant empirical modes, Phys. Rev. E **67**, 056312 (2003).
[22] P. A. Stone, A. Roy, R. G. Larson, F. Waleffe, and M. D. Graham, Polymer drag reduction in exact coherent structures of plane shear flow, Phys. Fluids **16**, 3470 (2004).
[23] L. Xi and M. D. Graham, Active and Hibernating Turbulence in Minimal Channel Flow of Newtonian and Polymeric Fluids, Phys. Rev. Lett. **104**, 218301 (2010).
[24] C. F. Li, R. Sureshkumar, and B. Khomami, Influence of rheological parameters on polymer induced turbulent drag reduction, J. Non-Newtonian Fluid Mech. **140**, 23 (2006).
[25] T. Vaithianathan, A. Robert, J. G. Brasseur, and L. R. Collins, An improved algorithm for simulating three-dimensional, viscoelastic turbulence, J. Non-Newtonian Fluid Mech. **140**, 3 (2006).
[26] W.-H. Cai, F.-C. Li, and H.-N. Zhang, DNS study of decaying homogeneous isotropic turbulence with polymer additives, J. Fluid Mech. **665**, 334 (2010).

[27] P. C. Valente, C. B. da Silva, and F. T. Pinho, The effect of viscoelasticity on the turbulent kinetic energy cascade, J. Fluid Mech. **760**, 39 (2014).
[28] P. O. Ferreira, F. T. Pinho, and C. B. da Silva, Large-eddy simulations of forced isotropic turbulence with viscoelastic fluids described by the FENE-P model, Phys. Fluids **28**, 125104 (2016).
[29] A. Kurganov and E. Tadmor, New high-resolution central schemes for nonlinear conservation laws and convection-diffusion equations, J. Comput. Phys. **160**, 241 (2000).
[30] T. Min, J. Yul Yoo, and H. Choi, Effect of spatial discretization schemes on numerical solutions of viscoelastic fluid flows, J. Non-Newtonian Fluid Mech. **100**, 27 (2001).
[31] G. K. Batchelor, Small-scale variation of convected quantities like temperature in turbulent fluid Part 1. General discussion and the case of small conductivity, J. Fluid Mech. **5**, 113 (1959).
[32] G. K. Batchelor, Small-scale variation of convected quantities like temperature in turbulent fluid Part 2. The case of large conductivity, J. Fluid Mech. **5**, 134 (1959).
[33] See Supplemental Material at http://link.aps.org/supplemental/10.1103/PhysRevFluids.3.011301 for additional numerical analyses demonstrating the adequacy of the numerical methodology and the quality of simulation results.
[34] P. J. Schmid and D. S. Henningson, *Stability and Transition in Shear Flows*, Vol. 142 (Springer Science & Business Media, 2012).
[35] L. Xi and M. D. Graham, Turbulent drag reduction and multistage transitions in viscoelastic minimal flow units, J. Fluid Mech. **647**, 421 (2010).
[36] L. Xi and M. D. Graham, Dynamics on the Laminar-Turbulent Boundary and the Origin of the Maximum Drag Reduction Asymptote, Phys. Rev. Lett. **108**, 028301 (2012).
[37] M. Zhang, I. Lashgari, T. A. Zaki, and L. Brandt, Linear stability analysis of channel flow of viscoelastic Oldroyd-B and FENE-P fluids, J. Fluid Mech. **737**, 249 (2013).
[38] O. Desjardins, G. Blanquart, G. Balarac, and H. Pitsch, High order conservative finite difference scheme for variable density low Mach number turbulent flows, J. Comput. Phys. **227**, 7125 (2008).
[39] Y. Morinishi, T. S. Lund, O. V. Vasilyev, and P. Moin, Fully conservative higher order finite difference schemes for incompressible flow, J. Comput. Phys. **143**, 90 (1998).
[40] J. Kim and P. Moin, Application of a fractional-step method to incompressible Navier-Stokes equations, J. Comput. Phys. **59**, 308 (1985).
[41] J. Jiménez and P. Moin, The minimal flow unit in near-wall turbulence, J. Fluid Mech. **225**, 213 (1991).
[42] Y. Dubief and F. Delcayre, On coherent-vortex identification in turbulence, J. Turbul. **1**, N11 (2000).
[43] S.-N. Wang, M. D. Graham, F. J. Hahn, and L. Xi, Time-series and extended Karhunen-Loève analysis of turbulent drag reduction in polymer solutions, AIChE J. **60**, 1460 (2014).
[44] S.-N. Wang, A. Shekar, and M. D. Graham, Spatiotemporal dynamics of viscoelastic turbulence in transitional channel flow, J. Non-Newtonian Fluid Mech. **244**, 104 (2017).